

Three-dimensional imaging of chemical bond orientation in liquid crystals by coherent anti-Stokes Raman scattering microscopy

Brian G. Saar¹, Heung-Shik Park², X. Sunney Xie¹, and Oleg D. Lavrentovich^{2,*}

¹Department of Chemistry and Chemical Biology, Harvard University, Cambridge, MA 02138

²Liquid Crystal Institute and Chemical Physics Program, Kent State University, Kent, OH 44242

*Corresponding author: odl@lci.kent.edu

Abstract: Liquid crystals are a class of industrially important materials whose optical properties make them useful particularly in display technology. Optical imaging of these materials provides information about their structure and physical properties. Coherent anti-Stokes Raman scattering (CARS) microscopy is used to provide three-dimensional chemical maps of liquid crystalline samples without the use of external labels. CARS is an optical imaging technique that derives contrast from Raman-active molecular vibrations in the sample. Compared to many other three-dimensional imaging techniques, CARS offers more rapid chemical characterization without the use of external dyes or contrast agents. The use of CARS to image chemical and orientational order in liquid crystals is demonstrated using several examples, and the limitations and benefits are discussed.

©2007 Optical Society of America

OCIS codes: (160.3710) Liquid crystals; (180.4315) Nonlinear microscopy; (300.6230) Spectroscopy, coherent anti-Stokes Raman scattering; (300.6450) Spectroscopy, Raman; (180.6900) Three-dimensional microscopy.

References and links

1. N. H. Hartshorn, *The Microscopy of Liquid Crystals* (Microscope Publications, London, 1974).
2. J. M. Haudin, in *Optical Properties of Polymers*, G. H. Meeten, ed., (Elsevier, Essex, 1986).
3. J. R. Bellare, H. T. Davis, W. G. Miller, and L. E. Scriven, "Polarized Optical Microscopy of Anisotropic Media: Imaging, Theory and Simulations," *J. Colloid Interface Sci.* **136**, 305-326 (1990).
4. M. Kleman, and O. D. Lavrentovich, *Soft Matter Physics: An Introduction* (Springer, New York, 2003).
5. K. Kaznacheev and T. Hegmann, "Molecular ordering in biaxial smectic-A phase studied by scanning transmission X-ray microscopy (STXM)," *Phys. Chem. Chem. Phys.* **9**, 1705-1712 (2007).
6. I. I. Smalyukh, S. V. Shiyankovskii, and O. D. Lavrentovich, "Three-dimensional imaging of orientational order by fluorescence confocal polarizing microscopy," *Chem. Phys. Lett.* **336**, 88-96 (2001).
7. R. S. Pillai, M. Oh-e, H. Yokoyama, G. J. Brakenhoff, and M. Müller, "Imaging colloidal particle induced topological defects in a nematic liquid crystal using third harmonic generation microscopy," *Opt. Express* **14**, 12976-12983 (2006).
8. D. Yelin, Y. Silberberg, Y. Barad, and J. S. Patel, "Phase-Matched Third-Harmonic Generation in a Nematic Liquid Crystal Cell," *Phys. Rev. Lett.* **82**, 3046 (1999).
9. D. Yelin, Y. Silberberg, Y. Barad, and J. S. Patel, "Depth-resolved imaging of nematic liquid crystals by third-harmonic microscopy," *Appl. Phys. Lett.* **74**, 3107-3109 (1999).
10. M. Ofuji, Y. Takano, Y. Houkawa, Y. Takanishi, K. Ishikawa, H. Takezoe, T. Mori, M. Goh, S. Guo, and K. Akagi, "Microscopic orientational order of polymer chains in helical polyacetylene thin films studied by confocal laser Raman microscopy," *Jpn. J. Appl. Phys.* **45**, 1710-1713 (2006).
11. E. A. Buyuktanir, K. Zhang, A. Gericke, and J. L. West, "Raman mapping of the orientation of nematic and smectic liquid crystals," in *21st International Liquid Crystal Conference* (Keystone, CO, 2006), pp. DFCTP-25.
12. J. F. Blach, M. Warengem, and D. Bormann, "Probing thick uniaxial birefringent medium in confined geometry: A polarised confocal micro-Raman approach," *Vib. Spectrosc.* **41**, 48-58 (2006).
13. P. Camorani, and M. P. Fontana, "Local three-dimensional characterization of a micro-patterned liquid crystalline cell by confocal Raman microscopy," *Mol. Cryst. Liq. Cryst.* **465**, 143 - 152 (2007).
14. J. X. Cheng and X. S. Xie, "Coherent anti-Stokes Raman scattering microscopy: instrumentation, theory, and applications," *J. Phys. Chem. B* **108**, 827-840 (2004).

15. C. L. Evans, E. O. Potma, M. Puoris'haag, D. Côté, C. P. Lin, and X. S. Xie, "Chemical imaging of tissue *in vivo* with video-rate coherent anti-Stokes Raman scattering microscopy," *P. Natl. Acad. Sci. USA* **102**, 16807-16812 (2005).
16. X. Nan, E. O. Potma, and X. S. Xie, "Nonperturbative chemical imaging of organelle transport in living cells with coherent anti-Stokes Raman scattering microscopy," *Biophys. J.* **91**, 728-735 (2006).
17. T. B. Huff, and J. X. Cheng, "In vivo coherent anti-Stokes Raman scattering imaging of sciatic nerve tissue," *J. Microsc.* **225**, 175-182 (2007).
18. E. O. Potma, X. S. Xie, L. Muntean, J. Preusser, D. Jones, J. Ye, S. R. Leone, W. D. Hinsberg, and W. Schade, "Chemical imaging of photoresists with coherent anti-Stokes Raman scattering (CARS) microscopy," *J. Phys. Chem. B* **108**, 1296-1301 (2004).
19. G. W. H. Wurpel, H. A. Rinia, and M. Müller, "Imaging orientational order and lipid density in multilamellar vesicles with multiplex CARS microscopy," *J. Microsc.* **218**, 37-45 (2005).
20. H. Kano and H. Hamaguchi, "Three-dimensional vibrational imaging of a microcrystalline J-aggregate using supercontinuum-based ultra-broadband multiplex coherent anti-Stokes Raman scattering microscopy," *J. Phys. Chem. B* **110**, 3120-3126 (2006).
21. G. W. H. Wurpel and M. Müller, "Water confined by lipid bilayers: A multiplex CARS study," *Chem. Phys. Lett.* **425**, 336-341 (2006).
22. W. J. Jones, "Picosecond inverse Raman spectroscopy of liquid crystals," *J. Mol. Struct.* **404**, 129-136 (1997).
23. I.-C. Khoo, *Liquid Crystals: Physical Properties and Nonlinear Optical Phenomena* (Wiley-Interscience, New Jersey, 1994).
24. V. A. Enikeeva, V. A. Makarov, I. A. Ozheredov, A. P. Shkurinov, I. A. Budagovsky, V. F. Kitaeva, Zolot, apos, A. S. ko, and M. I. Barnik, "Orienting influence of femtosecond pulses on nematic liquid crystals," *Mol. Cryst. Liq. Cryst.* **442**, 1 - 18 (2005).
25. L. M. Blinov, and V. G. Chigrinov, *Electrooptic Effects in Liquid Crystal Materials* (Springer, New York, 1994).
26. W. J. Jones, D. K. Thomas, D. W. Thomas, and G. Williams. "Raman scattering studies of homogenous and twisted-nematic liquid crystal cells and the determination of $\langle P_2 \rangle$ and $\langle P_4 \rangle$ order parameters." *J. Mol. Struct.* **614**, 75-85, (2002).
27. E. V. Astrova, T. S. Perova, S. A. Grudinkin, V. A. Tolmachev, Y. A. Pilyugina, V. B. Voronkov, and J. K. Viji, "Polarized infrared and Raman spectroscopic studies of the liquid crystal E7 alignment in composites based on grooved silicon." *Semiconductors.* **39**, 759-767, (2005).
28. J.-X. Cheng, L. D. Book, and X. S. Xie, "Polarization coherent anti-Stokes Raman scattering microscopy," *Opt. Lett.* **26**, 1341-1343 (2001).

1. Introduction

Orientalional order is a salient feature of many soft matter systems, ranging from low-molecular weight thermotropic liquid crystals used in display technology to condensed phases of biopolymers such as DNA and f-actin. Observing the behavior of these ordered systems and how they respond under various conditions (*e.g.* temperature, pressure, applied electric fields, etc.) is critical to understanding their physics and to designing improved materials.

Much of the modern understanding of orientational order in these systems has been discovered through optical microscopy. Many optical imaging tools have been applied to liquid crystals. Perhaps the most widely used technique to characterize ordered materials is polarizing light microscopy (PM). PM tests the orientation of the optic axes that are related to the pattern of orientational order.[1-4] However, a PM image carries only two-dimensional (2D) information, as the 3D pattern of optical birefringence is integrated over the path of light.[3] Another recently presented technique, scanning transmission x-ray microscopy, offers higher spatial resolution than PM but is still limited to two-dimensional information.[5] Three dimensional imaging of orientational order has been achieved with fluorescence confocal polarizing microscopy (FCPM).[6] In FCPM, the sample is doped with anisometric fluorescent dye molecules that are aligned by the ordered matrix. The sample is scanned with a focused polarized beam and the average director orientation $\hat{\mathbf{n}}(\mathbf{r})$ is deduced from the intensity of fluorescence that depends on the mutual directions of polarization of probing light and the transition dipole \mathbf{d} (related to the director of the orientational order, usually as $\mathbf{d} \parallel \hat{\mathbf{n}}$) of the dye. This technique requires a chemical perturbation to the sample, though typically a low dye concentration may be used.

Recently, two techniques have been demonstrated which provide non-perturbative imaging of liquid crystals in three dimensions. Pillai *et al.*[7] built on the previous work of Yelin *et al.*[8, 9] to use third harmonic generation (THG) microscopy to image director

distortions induced by colloidal particles in a liquid crystal. In THG imaging, the contrast is based both on changes in the material's nonlinear susceptibility at the laser focus and on the local orientation of the director relative to the laser polarization, but it does not offer any direct chemical information. THG has been shown to be sensitive to the birefringence induced by the liquid crystalline materials, but the weak signal strength requires relatively long pixel dwell times (>50 ms at the average powers used in that study), making characterization of samples in a wide range of conditions a time-consuming process, and making fast dynamics impossible to observe.

Another promising tool to image orientational order is confocal Raman microscopy. This technique allows for three-dimensional imaging that is both chemically selective and non-invasive. In Raman microspectroscopy, chemical information is acquired by dispersing the inelastically scattered light from the sample onto a detector. The frequency/wavelength shifts from the monochromatic pump wavelength correspond to the natural frequencies of vibration of individual chemical groups within the molecule. For example, Ofuji *et al.*[10] used Raman microscopy to image solid films of orientationally ordered fibrils in polyacetylene films with contrast based on the C=C bond stretching frequency, while Buyuktanir *et al.*[11] used the cyano (CN) group stretching frequency to image defects in liquid crystal samples. Blach *et al.*[12] developed a theory of polarized Raman microscopy in a birefringent medium and probed the director by using the vibrational mode at 2226 cm^{-1} . Camorani and Fontana used polarization sensitive confocal Raman microscopy to characterize liquid crystal alignment at a micropatterned substrate.[13] In general, Raman spectroscopy offers a wealth of chemical information but usually at the cost of relatively long integration times (100-200 ms per pixel in the work above), restricting its application to static samples.

An ideal optical imaging technique for imaging liquid crystalline samples would have the following properties:

1. Three-dimensional imaging of the orientational order of the sample.
2. Minimal sample perturbation: no labels should be added, and the interaction of the probing light with the sample should not reorient the sample.
3. Rapid imaging, to allow either visualization of sample dynamics or characterization under a range of experimental conditions in a reasonable amount of time.
4. The ability to image the degree of order of the various chemical constituents of the sample.

In this work, we demonstrate that all of the above requirements for 3D imaging of orientational order of pre-selected chemical bonds can be satisfied by using laser-scanning coherent anti-Stokes Raman scattering (CARS) microscopy.[14] In the CARS process [Fig. 1(a)], the sample is excited with laser light at two optical frequencies, called the "pump" (ω_p) and "Stokes" (ω_s). Upon excitation, the sample generates light at the "anti-Stokes" frequency, $\omega_{as}=2\omega_p-\omega_s$, through a four wave mixing process. When the difference frequency between the pump and Stokes, $\omega_p-\omega_s$, is tuned onto resonance with a molecular vibration in the sample, a large enhancement in the anti-Stokes intensity is observed. This is used as the contrast mechanism for microscopic imaging. For a nonlinear process, pulsed light sources are typically used to maximize signal generation efficiency. The CARS signal generated by a given material is related to its third order nonlinear susceptibility, $\chi^{(3)}$. $\chi_{apps}^{(3)}$ is a fourth rank tensor, whose four indices represent the polarization directions of the anti-Stokes, probe (the same as the pump in our experiment), pump and Stokes beams, respectively. In the most general case, $\chi^{(3)}$ can have $4^3=64$ unique elements, suggesting a large number of possible excitation and detection combinations for CARS. In this case, the pump and probe beams are derived from the same laser beam, and the Stokes is polarized parallel to the pump and probe polarization in the x-y plane of the image. The anti-Stokes is detected without discriminating based on the polarization. Thus the imaging of orientational order is detected primarily by the difference between $\chi_{xxxx}^{(3)}$ and $\chi_{yyyy}^{(3)}$ in this experiment

In practice [Fig. 1(b)], CARS imaging is implemented by combining the pump and Stokes pulse trains in time and space and focusing them through a high numerical aperture microscope objective (see methods). CARS signal is collected in either the forward or epi (backward) direction as the beams are raster scanned over the sample. Scan speeds of 4 μs per pixel are routinely used, though imaging at video rate (100 ns pixel dwell time) has also been demonstrated for CARS.[15] Because CARS is a nonlinear process, signal is only generated from the focal volume, which can be scanned in three dimensions. CARS microscopy thus offers three dimensional imaging with chemical selectivity using no external labels at a speed that is orders of magnitude faster than spontaneous Raman scattering or THG microscopy. CARS imaging has found numerous biological and biomedical applications[15-17], as well as several in materials science.[18-20] In this work, we demonstrate the benefits of CARS for imaging liquid crystals.

In this implementation of CARS, only a single molecular vibration is probed at a time, which allows for rapid image acquisition. Previously, it has been shown that careful understanding of the vibrational spectrum of a given sample is a crucial step in interpreting CARS images taken in congested spectral regions.[21] In this case, the Raman spectrum of the E7 liquid crystalline material [Fig. 1(c)] suggests a number of sharp, isolated features. For this work, the typical molecular groups frequently met in liquid crystalline materials were probed [Fig. 1(d)] by using the CN stretching (2215 cm^{-1}) and aryl stretching ($\sim 1600\text{ cm}^{-1}$) vibrations.[22] When imaging the sample far from any vibrational resonances, we observed minimal contrast due to the nonresonant four wave mixing background. In some biological samples, this nonresonant background can be overwhelmingly strong, reducing image contrast. In the liquid crystalline samples that we studied, the vibrational resonance enhancement is substantial and allows for high contrast chemical imaging without taking extra measures for background suppression.

Liquid crystals are media with a long-range orientational order of the constituent molecules (or aggregates) and partial or no positional order.[4] A classical example is the nematic (N) liquid crystal, in which the molecules are on average parallel to director \hat{n} but there is no positional order. A partial one-dimensional positional order is found in the smectic A (SmA) liquid crystal: the density is modulated along \hat{n} with a period usually close to the length of an individual molecule.[4] The director orientation can change from point to point in the sample, under an orienting action of the bounding plates, applied electric voltage, presence of defects, or other effects. Several examples of nematic and smectic A textures demonstrate the applicability of CARS microscopy to the studies of liquid crystals, namely, (a) planar monodomain N samples, (b) electrically-induced reorientation in the N bulk with depth-dependent director distortions, (c) Schlieren textures formed by line and point defects in the N phase, (d) SmA textures of so-called focal conic domains (FCDs).[4]

2. Materials and methods

2.1. Sample preparation

(a) *Nematic cells for monodomain and Frederiks transition studies.* Glass plates coated with transparent indium tin oxide (ITO) electrodes were rubbed with a metal bar coated with a cloth, at pressure 800-850 Pa, for a unidirectional planar alignment. The cell was assembled from two plates with the gap (20 ± 2) μm between them fixed by glass microspheres mixed with UV glue (Norland Products, Inc., Norland 65) at the cell edge. This gap was measured using the interference method and a spectrophotometer (Perkin Elmer, Lambda 18). The cell was filled with E7 (EMD Chemicals, Inc.). (b) *Cell for Schlieren textures.* The cells were prepared in a similar fashion, but the glass was not coated with ITO and was not rubbed. (c) *Smectic A cells.* The cells were prepared as in (b) but the gap thickness was $30\mu\text{m}$. The cell were filled with a 50 wt%:50wt% mixture of SmA octylcyanobiphenyl (8CB) and glycerol (Sigma-Aldrich).

2.2. CARS microscopy

To perform a CARS imaging experiment, we require pulsed lasers at two different wavelengths that are overlapped in space and synchronized in time. In this case, we use a passively mode-locked Nd:YVO₄ oscillator (High Q Laser, PicoTrain) which delivers a ~6 ps pulse train at 1064 and 532 nm with a repetition rate of 80 MHz. The 532 nm light (~4W) is used to synchronously pump an optical parametric oscillator (APE GmbH, Levante Emerald) based on a non-critically phase-matched lithium triborate (LBO) crystal. The signal wavelength of the OPO is tunable from 680-980 nm by adjusting the LBO temperature and is used as the pump wavelength for CARS. The idler wave is rejected with a short pass filter (Chroma Technology, 985SP). The signal beam is combined with the 1064 nm fundamental from the Nd:YVO₄ laser on a dichroic mirror (Chroma Technology, 1064DCRB). The combined beams are linearly polarized and can be rotated using an achromatic zero order $\lambda/2$ plate in the beam path (Thorlabs, AHWP05M-950) and attenuated to the desired power using a variable neutral density filter. The beams were then coupled into a modified laser scanning microscope (Olympus, FV300-IX71) and focused on the sample using a water immersion objective (Olympus UPlanSApo, NA 1.2, X60). The anti-Stokes light was detected in the forward direction on a non-descanned detector utilizing a photomultiplier tube (Hamamatsu, R9876) after filtering by optical filter sets (Chroma Technology, HQ710/100m-2p & E760SP or HQ750/210m). We found the following pump wavelengths to be optimal: 909.2 nm (aryl stretching), 861.0 nm (CN stretching), and 816.7 nm (CH stretching). Images were collected using commercial software (Olympus FluoView 5) at 1 frame/s (512x512 pixels). *XZ* stacks were created by scanning the objective in 450 nm increments with respect to the sample using a stepper motor. Images were processed using Igor Pro (Wavemetrics).

3. Imaging a planar nematic sample

We prepared an N monocrystal of the liquid crystal material E7 using two glass plates in a sandwich-type cell of thickness 20 μm . The CARS signal strength of the aligned E7 slab imaged at 2215 cm^{-1} corresponding to the CN group strongly depends on the polarization \mathbf{P} of the probing beams, reaching maximum when $\hat{\mathbf{n}} \parallel \mathbf{P}$ and minimum when $\hat{\mathbf{n}} \perp \mathbf{P}$. The ratio of the maximum signal to the minimum signal is ~10, indicating that the CN groups are well aligned along the director, as expected, because these groups are on average parallel to the long axes of elongated LC molecules [Fig. 1(d)]. Before further optical imaging on liquid crystalline samples, it was important to establish whether the torque imparted by the applied electric field of the laser beam can reorient the sample, perturbing the images through the optical Fredericks effect.[23] As shown by Enikeeva *et al.*, short-pulsed (femtosecond) laser irradiation causes director reorientation comparable to that caused by the CW irradiation at the same average power, suggesting that the pulse width is not the most critical parameter for this effect.[24] To address the issue directly, the beams were focused in the middle plane of the 20 μm E7 cell, i.e. at the location where the surface anchoring forces responsible for the uniform planar director orientation $\hat{\mathbf{n}}=(1,0,0)$ are the weakest. To impart a maximum torque, the light field was polarized at 45° with respect to the director. We recorded images for 100 s at average excitation powers of 16, 32 and 64 mW. 64 mW represents the highest average power used in any images in this study. We observed a change in the intensity recorded at the detector of less than +/-6% [Fig. 2(a)]. This intensity variation is consistent with the known CARS intensity fluctuations in our system. We therefore conclude that no substantial optical reorientation took place in our experiment.

The conclusion is supported by comparison with a previous experiments by Yelin *et al.*[9], performed for similar planar E7 cells and focused pulsed laser beams (130 fs, repetition rate 80 MHz, average power 100 mW, focused into a <1 μm spot). In these experiments, the director was reoriented by an angle $\alpha_{\text{max}} \approx \pm 10^\circ$ from the rubbing direction set at the bounding plates, requiring a time $\tau_{\text{max}} \approx 50$ ms to develop. Using this experimental finding as a reference, and assuming that for short times the dynamics of director deviation can be

approximated by a linear dependence on time [23], we can estimate the angle of director reorientation in CARS experiment as $\alpha \sim \alpha_{\max} \tau_{\text{dwell}} / \tau_{\max}$. Since the dwell time per pixel in CARS experiments is small ($\tau_{\text{dwell}} = 4 \mu\text{s}$ and thus $\tau_{\text{dwell}} / \tau_{\max} \sim 10^{-4}$), the director distortions are expected to be small, in accordance with the test above. The smallness of the dwell time in CARS microscopy represent a real advantage of the technique, not only in faster acquisition of data but, more importantly, in reducing the optically-induced director distortions as compared to techniques such as THG.[7]

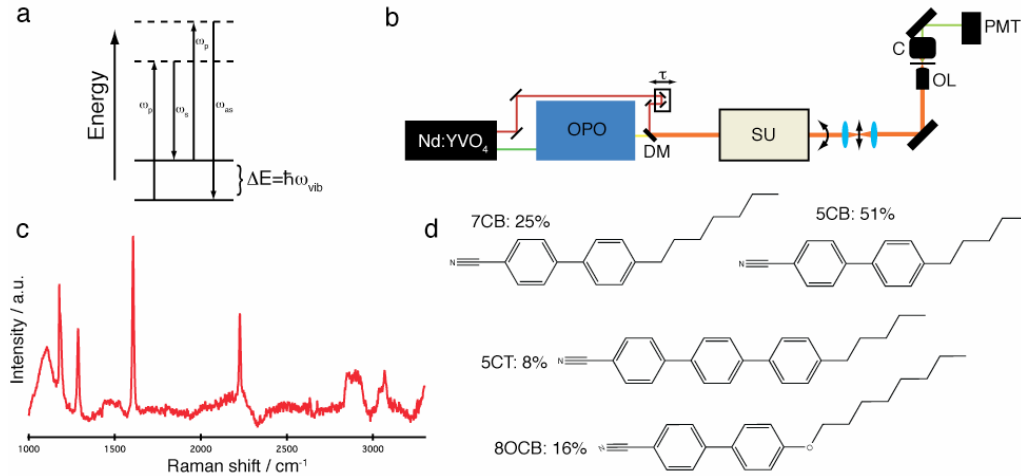


Fig. 1. CARS Microscopy of Liquid Crystals (a) Energy diagram for coherent anti-Stokes Raman scattering microscopy (b) Schematic of the CARS microscope. Nd:YVO₄: 1064 & 532 nm laser; OPO: optical parametric oscillator. DM: dichroic mirror; SU: microscope scan unit; OL: 1.2NA water X60 objective lens; C: 0.55 NA air condenser; PMT: photomultiplier tube. (c) Raman spectrum of the E7 liquid crystal, displaying strong peaks at 1600 cm⁻¹ and 2215 cm⁻¹. (d) Chemical composition of the E7 mixture.

4. Imaging of the Frederiks transition

Liquid crystals such as E7 are dielectrically anisotropic, so that a sufficiently strong external electric field can reorient $\hat{\mathbf{n}}$. The effect is called the Frederiks transition.[4] To observe a Frederiks transition, we applied a sine wave voltage at 1 kHz between the top and bottom glass plates coated with transparent Indium Tin Oxide (ITO) electrodes, so that the field is perpendicular to $\hat{\mathbf{n}}$. Since the dielectric anisotropy of E7 is positive, the applied field tends to reorient the director vertically, towards the state $\hat{\mathbf{n}}=(0,0,1)$ when the voltage is high. At small voltages, below the well-defined threshold, the structure remains uniform, $\hat{\mathbf{n}}=(1,0,0)$. Above this threshold, the electric field becomes strong enough to overcome the anchoring forces at the bounding plates and elasticity of the N sample to reorient $\hat{\mathbf{n}}$ from its strictly horizontal orientation, towards the Z-axis. The maximum deviation was observed in the middle of the cell, as predicted by theory [Fig. 2(b)].[25] We imaged the sample by recording *XY* images at 0.45 μm intervals along the Z direction, making use of contrast both at the CN stretching frequency (2215 cm⁻¹) and at the CH₂ stretching frequency (2845 cm⁻¹). We imaged the sample at a series of voltages: 0V, 2.5V, 5V and 8V. The *XZ* profiles of the sample are shown in Figs. 2(c) and 2(d). In Fig. 2(c), which shows contrast at the CN band, we observed the typical signature of a Frederiks transition: at 0V, the director lies along Z, and the sample shows a constant signal along the Z direction within the N phase and fades away once the probing beams move into the glass substrates. At 2.5V, the molecules in the center of the sample are re-oriented along Z and thus generate a decreased amount of CARS signal, yielding bands of intense signal only near the electrode boundaries, where $\hat{\mathbf{n}}$ remains horizontal or only slightly tilted. At even higher fields, the absolute signal level decreases as

the sample is increasingly oriented along Z and therefore generates less signal upon polarized excitation along X .

The results at the CH_2 stretching band [Fig. 2(d)] show a different behavior. At zero voltage, the signal is low compared to the CN band. At higher voltages, it decreases more slowly and does not show the banding observed in the CN images (*cf.* Figs. 2(c) and 2(d) at 2.5V). The CH trend, quite different from the one observed in the CN case, is understandable, since the CH_2 groups are on average roughly perpendicular to CN groups. However, the depth- and voltage-dependent contrast of the CH_2 signal is weaker than that of the CN signal; which can be attributed to the lower degree of orientational order of CH_2 groups that are associated with relatively flexible aliphatic tails of E7 molecules. This type of chemically-specific orientational information cannot be derived from fluorescence labeling or THG methods, and is unique to vibrational microscopy. A more detailed study of the contrast in different vibrational bands might yield further information about the degree of order of various chemical groups in liquid crystals.

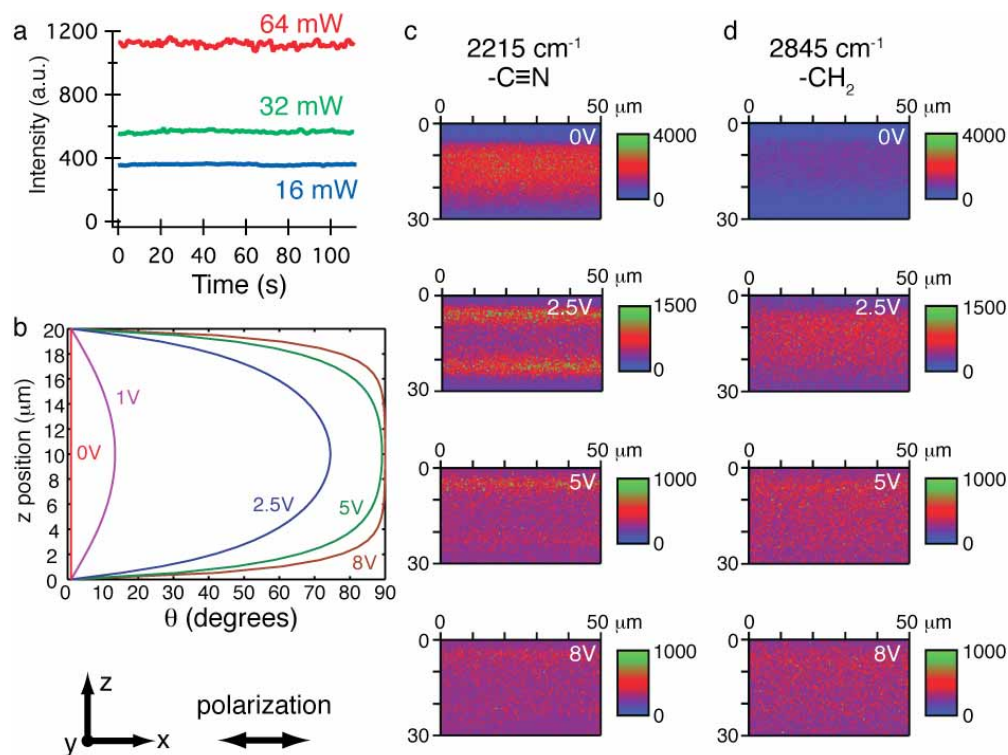


Fig. 2. Visualizing the Fredericks transition with CARS (a) CARS signal intensity over time, with the polarization at 45° to the director axis. No change in intensity is seen even at 64 mW average power, demonstrating that we do not optically re-orient the N sample. (b) Calculated average director angle as a function of Z -position for a $20\ \mu\text{m}$ thick E7 cell, at various applied voltages. (c) CARS depth profiles of the E7 cell tuned into the cyano stretch at $2215\ \text{cm}^{-1}$ at various voltages. The loss of signal in the center of the sample at elevated voltages is characteristic of a Fredericks transition, and demonstrates that the cyano groups (and the director) reorient vertically. (d) CARS images of the same sample at the alkyl stretching frequency of $2845\ \text{cm}^{-1}$. Different contrast and much less structure is observed, consistent with the fact that the CH groups are on average perpendicular to the director and associated with the flexible aliphatic chains in E7 molecules.

It is worth noting that FCPM gives information similar to that seen in the CN band image in Fig. 2(c). In the FCPM textures, the transition is also manifested by a reduced intensity of the fluorescence signal from the middle of the cell.[6] However, in FCPM, the sample must

be doped with a fluorescent dye, while CARS produces a similar depth-resolved information without labels. In addition to that, CARS offers the possibility of investigating fundamentally different types of order by tracing the spatial orientation of different chemical groups, including those parallel to the director and those perpendicular to it.

5. CARS of Schlieren textures

We also studied samples in which the bounding plates were not specially treated and provided a tangential orientation of the director, $\hat{\mathbf{n}} = (n_x, n_y, 0)$ without setting a preferred orientation in the XY plane. Figs. 3(a)-3(d) show typical intensity maps of the texture for the aryl group. The maximum CARS signal corresponds to the regions with $\hat{\mathbf{n}} \parallel \hat{\mathbf{P}}$ and minimum to $\hat{\mathbf{n}} \perp \hat{\mathbf{P}}$. The most prominent features are so-called disclination lines around which the director reorients by an angle $\pm\pi$ when one circumnavigates the core of defect once and point defects with director rotations by $\pm 2\pi$. Figures 3(a) - 3(d) and Fig. 3(h) illustrate the horizontal and vertical slices, respectively, of a N sample with a vertical disclination line [marked by a cross in Fig. 3(a)] whose two ends are located underneath each other at the opposite plates. The director reorientation by $\pm\pi$ is seen clearly as the disclination core separates the regions of maximum CARS signal from the minimum CARS signal. By rotating the linear polarization of the pump and Stokes beams together and making map of the regions with $\hat{\mathbf{n}} \parallel \hat{\mathbf{P}}$, one can reconstruct the entire director configuration. Figure 3(e) shows in-plane director configuration within the area limited by a rectangle in Fig. 3(a), around the point defect with a core marked by a circle.

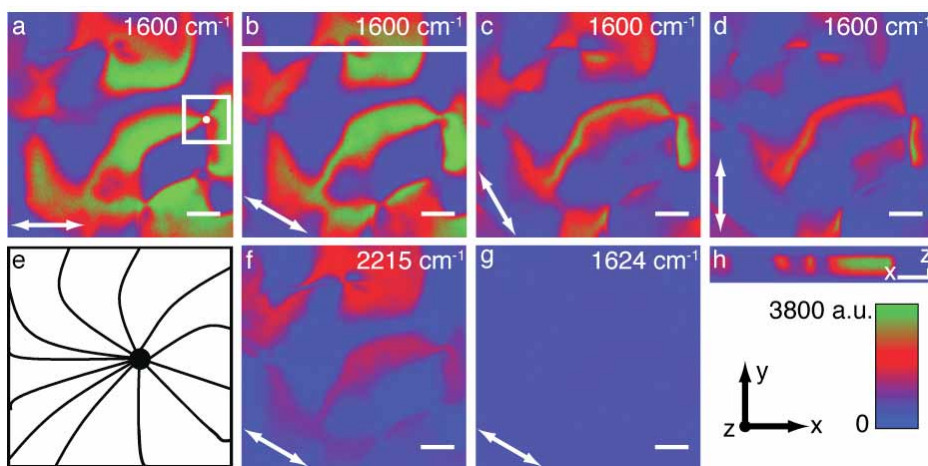


Fig. 3. CARS images of a Schlieren texture (a)-(d) Images at the aryl stretch at 1600 cm^{-1} , with the excitation beams polarized along the direction indicated by the double-headed arrow. All scale bars are $20\text{ }\mu\text{m}$. (e) sketch of the director field around a point defect (marked by a circle), based on data from (a)-(d). (f) CARS image at the cyano stretching band at 2215 cm^{-1} at the indicated polarization. (g) CARS image off resonance, showing minimal contrast at the same detector gain as in (a)-(d) and (f). (h) CARS depth profile along the Z axis taken down the line indicated in (b). X scale bar is $20\text{ }\mu\text{m}$, Z is $5\text{ }\mu\text{m}$.

We used the same Schlieren texture to illustrate the resonance enhancement of CARS at two bands of interest. In Figs. 3(a)-3(e), the orientation of the vibrations corresponding to the aromatic functionality of the molecules in Fig. 1(d) are mapped. In Fig. 3(f), a similar map is produced for the CN vibrations at 2215 cm^{-1} ; the contrast is somewhat lower than in the aromatic band. By tuning the pump laser to a Raman shift of 1624 cm^{-1} (a shift of $\sim 2\text{ nm}$ from the 1600 cm^{-1} aryl band) but keeping the excitation power unchanged, we observe that the contrast is decreased by more than an order of magnitude ([fig. 3(g)], making the structure almost indistinguishable. By dividing Fig. 3(b) by 3(g), enhancement factors due to the

Raman resonance are calculated. In this case, a maximum enhancement of 13 is observed, and an average value of 8.4 ± 1.3 is observed over an area of $20 \times 10 \mu\text{m}$. This implies that the majority of our signal is due to the resonant part of the third order nonlinear susceptibility. Fig. 3(h) shows an XZ scan along the line indicated in Fig. 3(b), again demonstrating the capability of CARS to image molecular orientation with chemical selectivity in three dimensions.

The textures obtained for the same polarization direction in Figs. 3(b) and 3(f) are almost identical, indicating that the direction of the polarizability in both cases are nearly parallel to each other. This is consistent with literature Raman spectroscopy measurements [26, 27], which have also indicated that the polarizability of the aryl and cyano modes in the cyanobiphenyl structure lies along the director axis of the liquid crystal.

6. Imaging of smectic A liquid crystal/glycerol mixtures

Lamellar phases such as SmA often organize in distorted FCD structures in which the molecular layers are bent but remain parallel to each other. The layers adopt the shape of Dupin cyclides: surfaces whose lines of curvature are circles. A family of Dupin cyclides is associated with a pair of confocal hyperbola and ellipse, located in two mutually perpendicular planes.[4] The layers fold around the ellipse and the hyperbola in such a way that they remain perpendicular to the straight lines that connect any point on the ellipse to any point on the hyperbola. These straight lines are simultaneously the director \hat{n} and local optical axes.[1, 4]

To produce and observe the FCDs, we assembled $30 \mu\text{m}$ thick SmA cells with two transparent glass plates treated with a thin film of glycerol for tangential orientation of the director. The cells were filled with a 50wt%:50wt% mixture of SmA and glycerol. The texture in Fig. 4 shows a large portion of SmA in the top third and small inclusions of SmA in the bottom half surrounded by glycerol. The material was octylcyanobiphenyl (8CB), which has an SmA phase at room temperature.

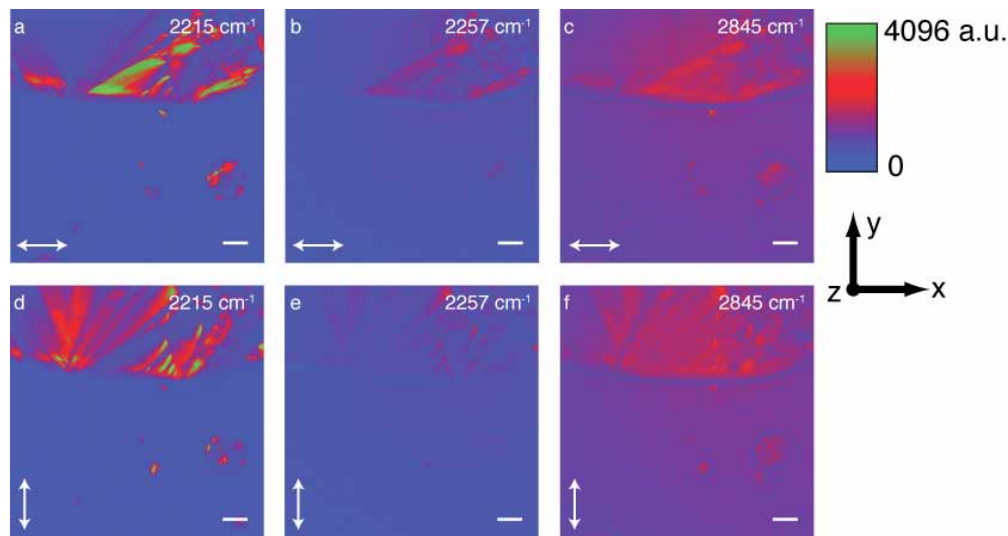


Fig. 4. Smectic texture imaged with CARS. Images are acquired of a smectic liquid crystal at the indicated vibrational difference frequency, with (a,d) cyano at 2215, (b,e) off resonance at 2257 and (c,f) alkyl at 2845 cm^{-1} . The scale bar is $20 \mu\text{m}$ in each image, and the polarization is along the direction indicated by the double-headed arrow. We observe a strong polarization dependence in the FCDs, with the strongest contrast in these images occurring at the cyano stretching region. Consistent with our results in Fig. 2, we observe less polarization dependence in the CH stretching region.

Figures 4(a) and 4(d) show CARS textures of XY optical slices of thickness $\sim 1 \mu\text{m}$ taken near one of the plates of the cell at the CN stretching Raman shift of 2215 cm^{-1} . This plane contains the elliptical bases of FCDs. Again, the maximum intensity of the anti-Stokes light occurs in the regions where $\hat{\mathbf{n}} \parallel \mathbf{P}$. By rotating the polarization, we are able to reconstruct the whole director pattern in the plane of the ellipse that is radial with a center in one of the foci of the elliptical base [4] (data not shown). In PM, a texture would show extinction whenever $\hat{\mathbf{n}}$ is along the polarizer *or* analyzer direction.[1, 3] Because of this degeneracy, PM does not distinguish readily two complementary director structures that are mutually orthogonal. In this case, one must perform additional measurements, using a compensating plate, but these additional measurements are practical only for specimen of certain (usually small, a few micrometers) thickness. CARS microscopy, (like FCPM [4, 6]) does not suffer from this type of degeneracy. In addition, we note that the degree of contrast is dependent on the chemical shift probed. In Figs. 4(b) and (e), we imaged the same SmA sample far from vibrational resonance at 2257 cm^{-1} . In that case, we observe a similar image to the CN band with much lower contrast. The maximum enhancement at a point is observed to be about 12. An average enhancement of 4.6 ± 1.4 is observed over a $20 \times 10 \mu\text{m}$ area in the image by dividing Fig. 4(a) by 4(b). The residual contrast in Fig. 4(b) is due to the nonresonant background, which in this case is higher than in Fig. 3(g). When tuning $\omega_p - \omega_s$ to the CH stretching band, we also observe lower contrast which appears to be more delocalized across the sample, and to respond less strongly to polarization. This is consistent with our previous result on the Frederiks transition [Fig. 2(c) and 2(d)] in which we observed that the contrast in the CH stretching region appears to be less diagnostic of molecular ordering. We note that the glycerol region (the bottom halves of the images in Fig. 4) does not show a polarization preference for excitation, consistent with an isotropic nature of this medium. By imaging the sample at the same vibrational frequency using two different polarization geometries (I_x and I_y ; the subscript denotes the polarization of the pump, probe and Stokes, which are all parallel), the director orientation at each point can be deduced according to $\arctan(I_x/I_y)$ and the magnitude of the polarization at each point can be calculated using $(I_x - I_y)/(I_x + I_y)$. We can represent the ordering of the sample as a vector field (Fig. 5).

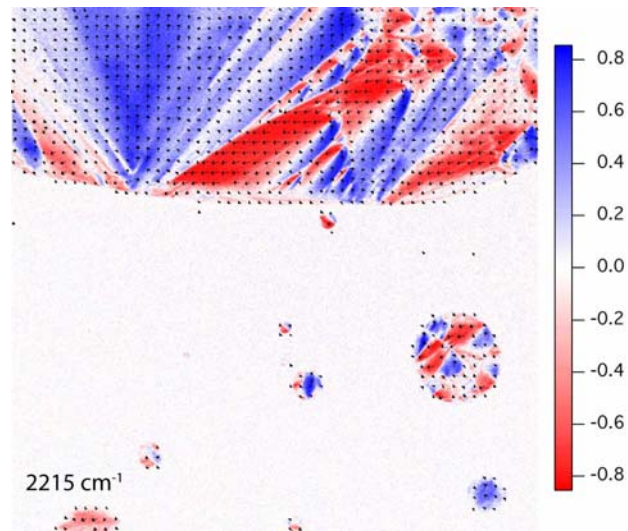


Fig. 5. Orientation map of the SmA liquid crystal. The background image shown in false color is a map of the polarization of the sample calculated according to $(I_x - I_y)/(I_x + I_y)$ using the images from Figs. 4(a) and 4(d). The overlaid vectors are obtained by smoothing the image using a 9 pixel \times 9 pixel moving average and then calculating the polarization angle and magnitude as described in the text. Vectors with polarization magnitude < 0.02 are not plotted for clarity. The majority of the vectors in the glycerol portion (bottom half) are therefore not plotted because the medium is isotropic.

7. Conclusion

Practical applications of CARS microscopy requires some care to avoid aberrations and other side effects. There are issues of common importance for both optically isotropic and anisotropic media as well as issues specific to ordered materials.

1. Optics of anisotropic medium. A focused laser beam of a sufficient power can cause director reorientation in the medium. In FCPM, the problem is not significant, since the power is usually less than 1 μW [6]. In CARS, the average power might be on the order of 10 mW-100mW and, in principle, the issue of director reorientation needs to be addressed. Our tests indicate that because of the short dwell time, the director distortions are not significant. Another issue is that focusing the laser beam in a birefringent medium, even if the director is not perturbed, is more complicated than in an isotropic medium since there are two propagating modes with different indices of refraction. To reduce the aberrations one can use a liquid crystal host with a low birefringence, Δn : the spatial separation of the focuses for the two modes is approximately $g\Delta n h / \bar{n}$, where \bar{n} is the average refractive index, h is the distance between the entry and focus in the liquid crystal cell, and g is the number of the order of unity (dependent on the sample orientation).[6]
2. Finite absorption. Fig. 2(c) & (d) clearly illustrate that the top and the bottom of the vertical slices of the CARS images are slightly asymmetric. The reason is losses across the sample, associated with absorption of the material and scattering. The effect can be verified by turning the sample upside down. Reducing the sample thickness or depth of scanning all help to mitigate the problem.
3. Adiabatic following of polarization. The well-known effect in the optics of liquid crystals is that the polarization of both ordinary and extraordinary waves follows the local orientation of the director in a twisted cell (the so-called Mauguine regime). This effect must be taken into account while interpreting the confocal images for nematic samples with twist deformations, especially when the twist scale is supra-micron and light propagates along the twist axis.
4. Polarization geometry. We used only one configuration of light polarization, when the pump and Stokes light are linearly polarized in one direction and rotated together. The anti-Stokes light was detected without discrimination based on polarization. Depending on the need, one can use many other polarization geometries, such as polarization sensitive detection to reduce the nonresonant background in CARS microscopy.[28] Additional work to study the various permutations of polarization of the pump, Stokes and anti-Stokes light will add more dimensions to CARS studies of liquid crystalline materials.

In summary, we have shown in this work that CARS microscopy offers a versatile tool for rapid, nonperturbative three-dimensional interrogation of media with orientational order. In addition, specific chemical information that can only be accessed through vibrational spectroscopy is available. CARS offers a number of advantages over existing characterization techniques such as PM, FCPM, THG and spontaneous Raman microscopy. In this work, we have demonstrated imaging of a number of important textures, but given the number of possible samples, detection schemes and experimental conditions, CARS will likely prove to be an invaluable tool for studying orientationally ordered materials, such as liquid crystals, for years to come.

Acknowledgments

We thank Dr. Conor L. Evans for helpful comments on the manuscript. B.G.S acknowledges support from the Army Research Office through an NDSEG fellowship. CARS microscopy development has been funded by National Science Foundation grant number DBI-0649892 to

X.S.X. ODL acknowledges the support of an NSF DMR grant 0504516, the W. M. Keck Foundation and a MURI AFOSR grant FA9550-06-1-0337.